Supporting Information

Hollow Multi-Shelled Structures of Co_3O_4 Dodecahedron with Unique Crystal Orientation for Enhanced Photocatalytic CO_2 Reduction

Li Wang[†, ‡, #], Jiawei Wan[‡, #], Yasong Zhao[†, ‡], Nailiang Yang[‡, &] and Dan Wang[†, ‡, &, *]

[†] School of Chemistry and Chemical Engineering, Harbin Institute of Technology, Harbin, 150001, P. R. China

[‡] State Key Laboratory of Biochemical Engineering, Institute of Process Engineering, Chinese Academy of Sciences, Beijing 100190, P. R. China

[&] University of Chinese Academy of Sciences, Beijing 100049, P. R. China

* Corresponding author: E-mail: danwang@ipe.ac.cn (D. Wang).

#These authors contributed equally to this work.

Experimental Section

Regents: All reagents used were of analytical grade and were used as received without any further purification. $Co{\cdot}(NO_3)_2{\cdot}6H_2O$ was purchased from Aladdin Reagent. Dimethyl imidazole was purchased from Aladdin Reagent. Carbon dioxide gas was supplied by Beijing Chengxin Shunxing Gas Raw Material Sales Co., Ltd. Ultrapure water with a resistivity of 18.2 MΩ was used in all experiments.

Synthesis of ZIF-67 crystal.: All the chemicals were directly used after purchased without further purification. In a typical synthesis of 700-800 nm ZIF-67, two solutions were first prepared by dissolving 7.50 mmol of $Co{\cdot}(NO_3)_2{\cdot}6H_2O$ and 32.3 mmol of 2-methylimidazole in mixed solution of 20 ml ethanol and 20 ml methanol. Then, the solution of 2-methylimidazole was quickly poured into the solution of $Co{\cdot}(NO_3)_2$ and the resultant mixed solution was aged for 24 h at room temperature. The purple precipitate was collected by centrifugation and dried at 70 °C for 8 h. The size of ZIF-67 particles can be easily modulated by varying the amount of 2-methylimidazole and the age temperature with other conditions unchanged. When the molar amount of dimethylimidazole is 16.1 mmol, ZIF-67 of 500-600 nm is obtained, and when the aging temperature is 40 °C, 2.5 μm ZIF-67 is obtained.

Synthesis of multi-shelled Co_3O_4: DS and TS Co_3O_4 HoMSs were obtained by annealing the as obtained 700-800 nm and 2.5 μm ZIF-67 in the air at 425 °C for 1 h with a ramp rate of 0.5 °C min^{-1}. QS Co_3O_4 HoMSs was obtained by annealing the as obtained 2.5 μm ZIF-67 under the gas condition (O_2:N_2=1:9) at 425 °C for 1 h with a ramp rate of 0.5 °C min^{-1}.

Synthesis of QS Co_3O_4 with the template CMS: 10 μm carbon microspheres were synthesized by dissolving 40 mg cobalt acetate and 2.7 g glucose in 30 ml deionized water, and then placing the solvent in a reaction vessel at 180 °C for 5 h. QS Co_3O_4 HoMSs were synthesized through STA (sequential templating approach) as described elsewhere[1] with 10 μm CMSs.

Photocatalytic test: In a typical CO_2 photocatalytic reduction process, 5 mg of sample was initially dispersed in deionized water and then the dispersions were dripped onto the quartz glass (2×2 cm^2). After natural drying in the air, the quartz glass and 0.5 mL deionized water were put in a 100 mL high pressure reactor equipped with a quartz glass on the top. The reaction system was vacuumed-treated for five times, then pumped by high-purity CO_2 (99.999%) to reach 3 MPa pressure with H_2O vapor to reach an atmospheric pressure. The

light source for the photocatalysis was a 200 W Xe lamp with a standard AM 1.5 filter and a 780 nm reflector, in which the light density was about 100 mW/cm^2 by calibrating with an NREL-calibrated Si solar cell. During the reaction, 10 uL product gases was extracted, injected into and analyzed by the online Shimadzu gas chromatography (GC-2014 ATFSPL, 230 C) equipping flame ionization detector (FID Porapak N, 3 mm×2 m) and thermal conductivity detector (TCD Molecular sieve 13 X, 3 mm×2 m).

Characterization: Transmission electron microscopy (TEM), high-resolution TEM (HRTEM) and selected area electron diffraction (SAED) were perfromed on a FEI Tecnai G2 F20 electron microscope operated at 200 KV with the software package for automated electron tomography, and the morphology was observed under Hitachi S-4800 electron scanning electron microscope (SEM). Powder X-ray diffraction (XRD) patterns were recorded on Panaltical X'Pert-pro MPD X-ray power diffractometer, using Cu Kα radiation (λ=1.54056 Å). UV-Vis spectra were recorded on a Hitachi Model U-4100 spectrophotometer, and the raw data was calculated by Kubelka-Munk model. The nitrogen adsorption-desorption isotherms under liquid nitrogen (-196 °C) were measured on a Quantochrom Autosorb-1 MP sorption analyzer with prior degassing under vacuμm. XPS data were corrected with reference to C 1s (284.8 eV). Mott-Schottky measurements, electrochemical impedence spectroscopy (EIS) and time-resolved photo-current behaviors were performed on the electrochemical workstation (CH Instrμments Ins.) in a 3-electrode configuration with the assembled photoelectrodes (hollow multi-shelled Co_3O_4 using ZIF-67 as the template) as the working electrode, the Pt slice as the counter electrode and the SCE as the reference electrode, and 0.1 M Na_2SO_4 solution was used as the electrolyte. For photo-current behaviors, a 300 Xelamp (FX-300, Beijing Perfectlight Technology Co. Ltd.) with the current of 13 A was the light source. Thermogravimetric analysis (TGA) was performed under atmospheric environment using a Netzsch TG209F3 TGA system. Fourier transform-infrared (FT-IR) spectroscopy was performed using a PerkinElmer Spectrμm One spectrometer.

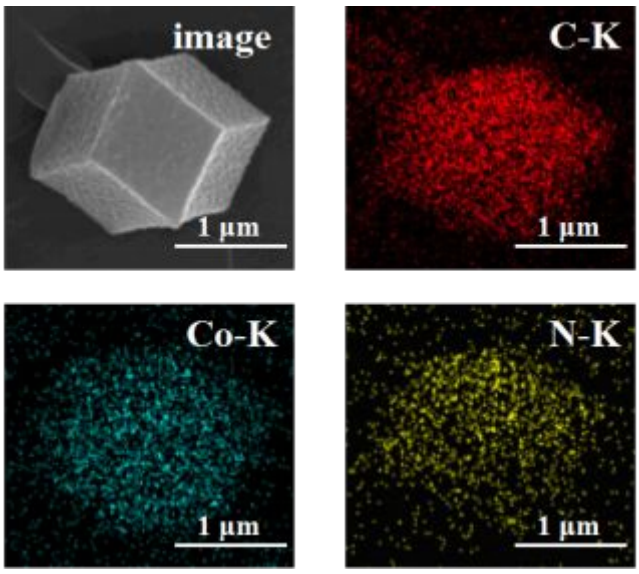

Fig S1. SEM mapping images of 2.5 μm ZIF-67.

Take 2.5 μm ZIF-67 as an example, Co, N, and C are distributed in the template uniformly.

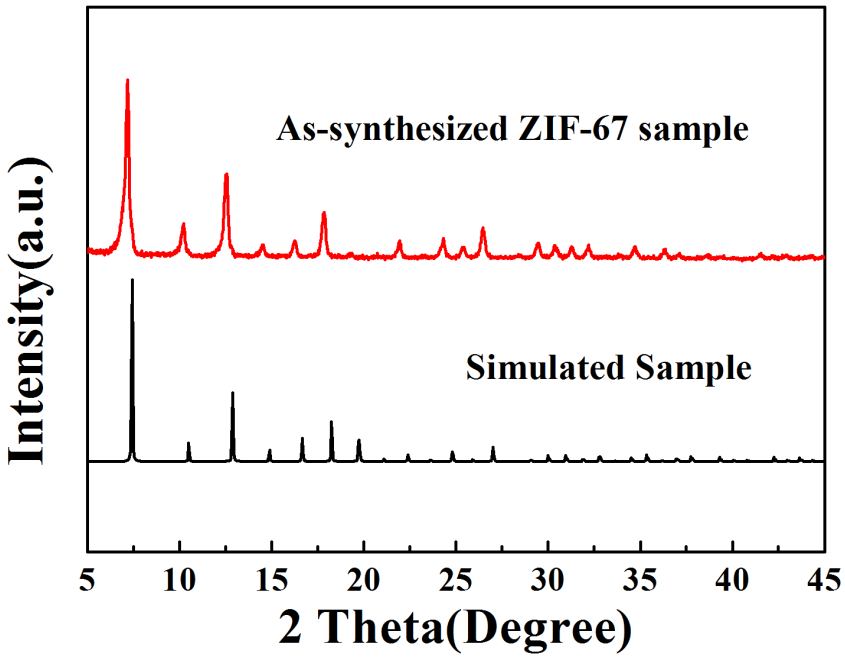

Figure S2. XRD patterns of simulated ZIF-67 and as-synthesized ZIF-67.

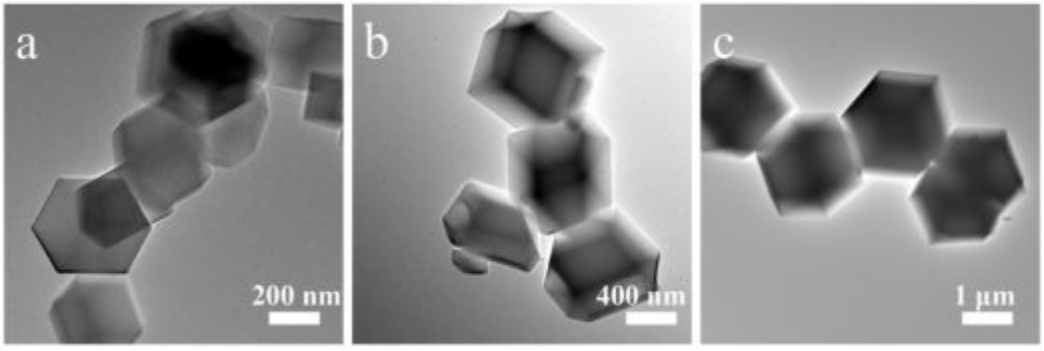

Figure S3. TEM images of (a) 400-500 nm ZIF-67, (b) 700-800 nm ZIF-67, (c) 2.5 μm ZIF-67.

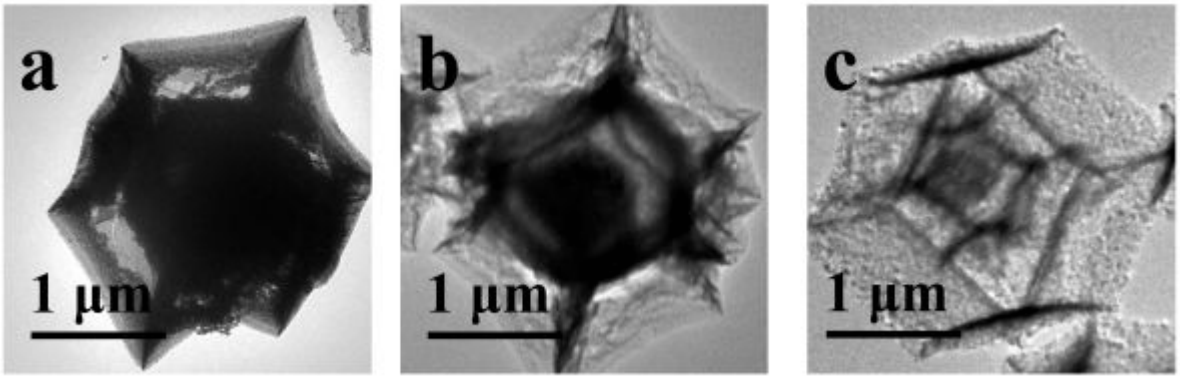

Figure S4. TEM images of 2 µm Co_3O_4 produced with different heating rate in the air at 425 °C for 1 h, (a) 10 °C/min, (b) 5 °C/min, (c) 0.5 °C/min.

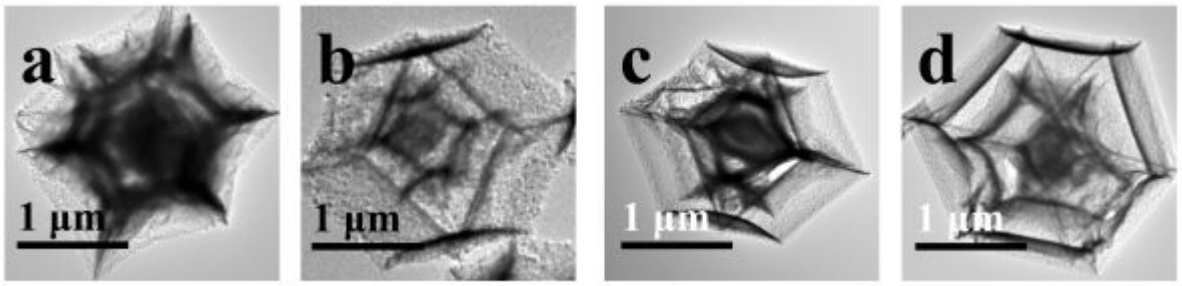

Figure S5. TEM images of 2 µm Co_3O_4 produced at 425 °C for 1 h with the heating rate of 0.5 °C/min under different gas conditions, O_2:N_2= (a) 1:1, (b) 1:4, (c) 1:9, (d) 1:19.

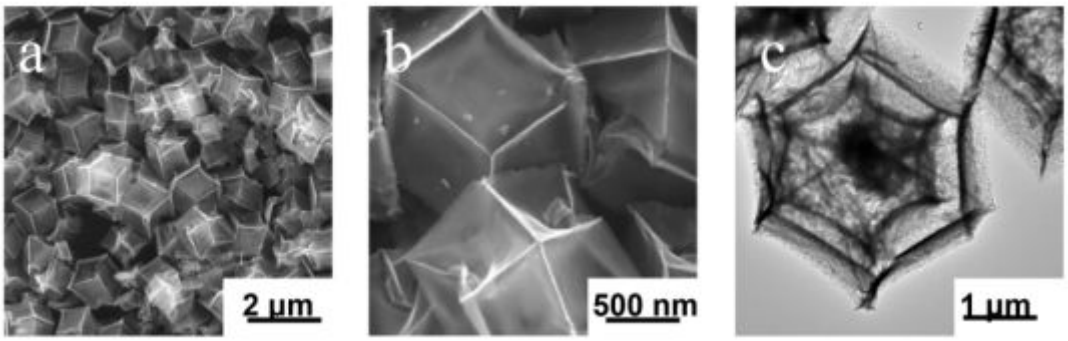

Figure S6. (a) SEM image, (b) magnified SEM image and (c)TEM image of TS-Co_3O_4 HoMSs.

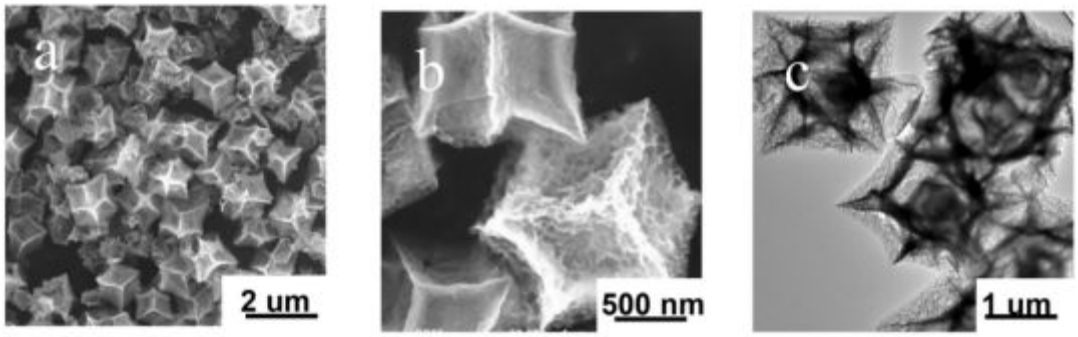

Figure S7. (a) SEM image, (b) magnified SEM image and (c)TEM image of QS-Co_3O_4 HoMSs.

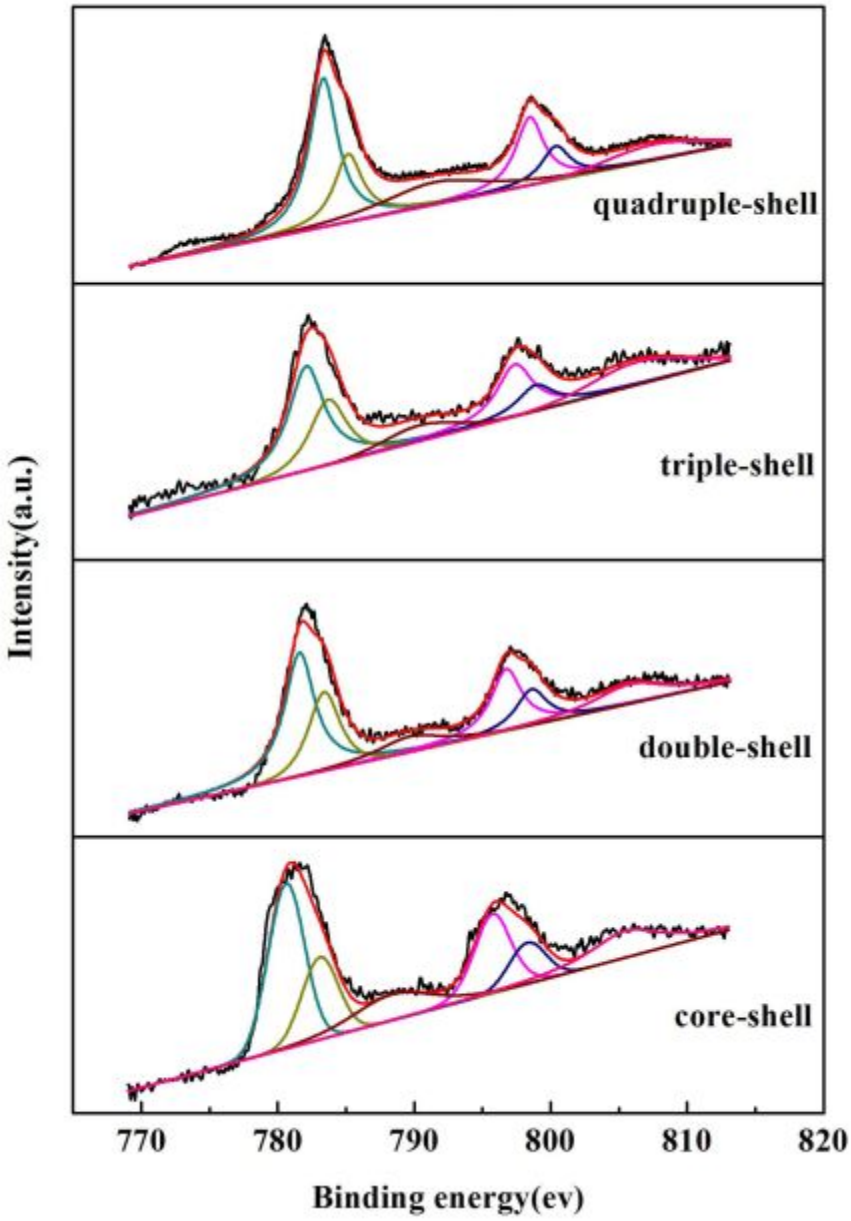

Figure S8. XPS spectra of CS, DS, TS and QS Co_3O_4 HoMSs (ZIF-67).

It can be observed from XPS spectra that there is no composition difference on the surface of CS, DS, TS and QS Co_3O_4 HoMSs (ZIF-67), and the peak area ratio of Co^{2+} and Co^{3+} are 1:2.

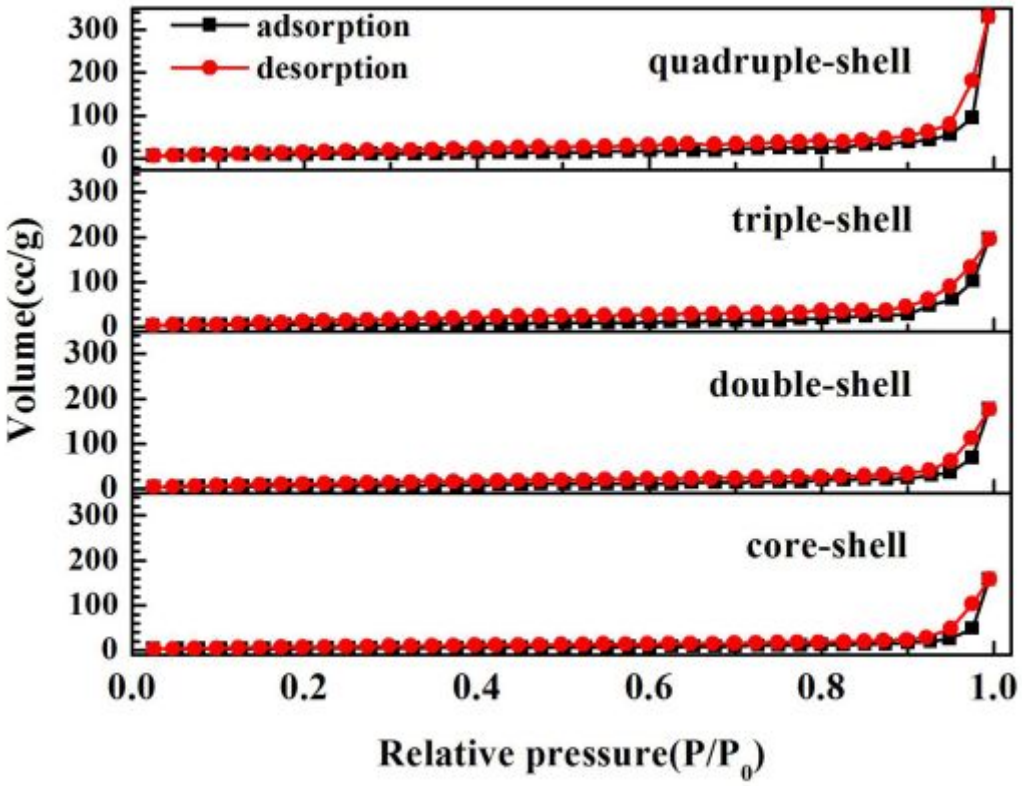

Figure S9. the N_2 adsorption–desorption isotherms of CS, DS, TS and QS Co_3O_4 HoMSs (ZIF-67).

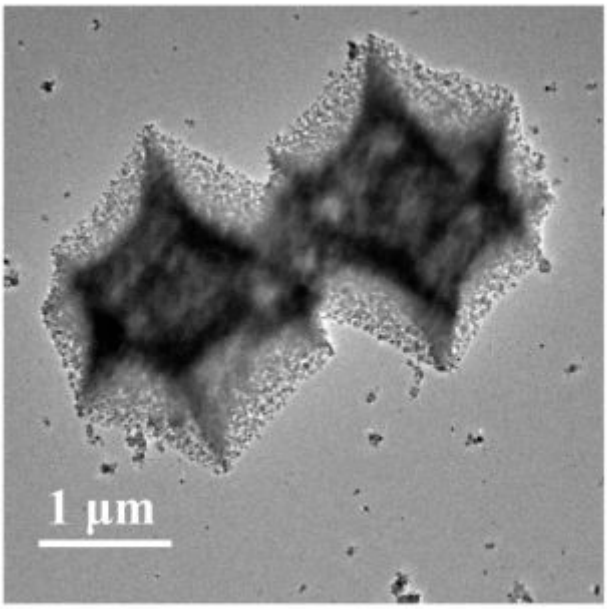

Figure S10. TEM image of sample producing by heating in N_2 with 2.5 μm ZIF-67 as the template.

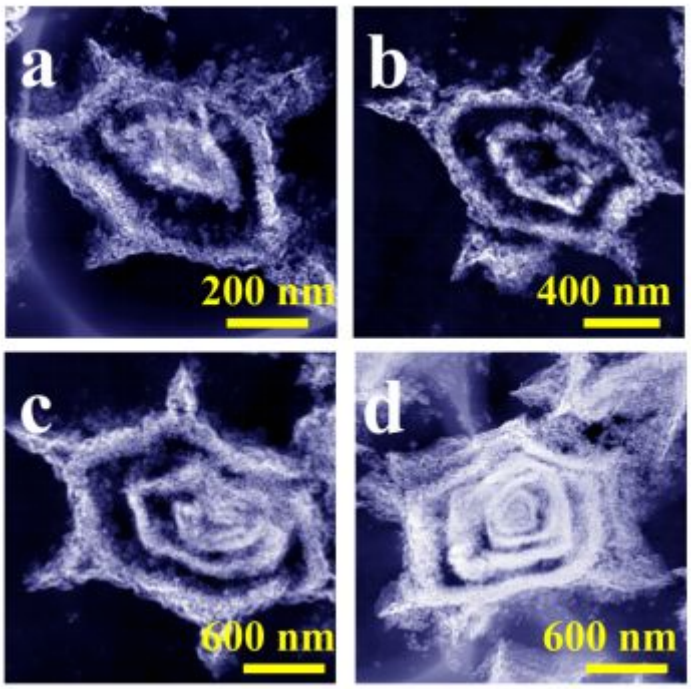

Figure S11. STEM images of the slice of (a) CS, (b) DS, (c)TS and (d) QS Co_3O_4 (ZIF-67).

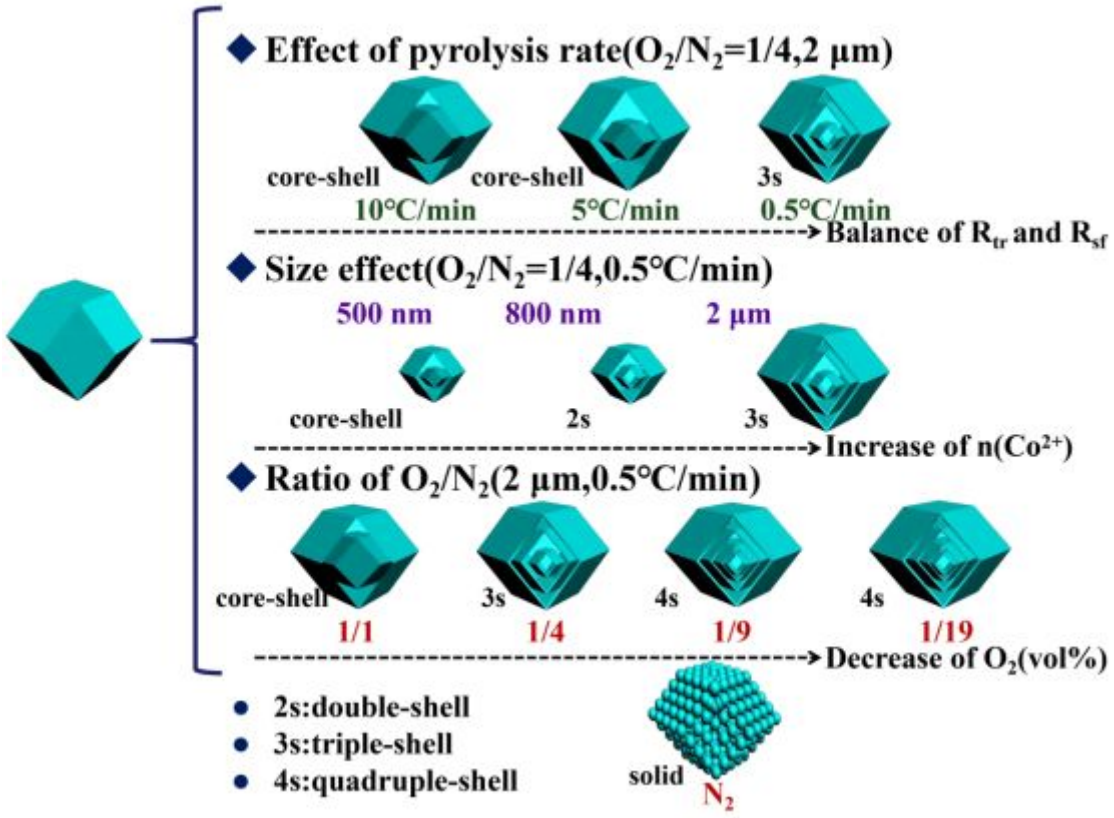

Figure S12. Scheme to illustrate the effect of synthesis conditions (heating rate, cobalt ion numbers in ZIF-67 and oxygen volume percentage in the gas) on shell formation.

First, the pyrolysis method of different heating rates was carried out. When the heating rate was 10 °C/min and 5 °C/min, CS HoMSs were obtained, and at 0.5 °C/min, it was TS HoMSs. When the heating rate is too fast, nanoparticles will agglomerate together to form a core. The most shell will be obtained only when the template removal rate Rtr matches with the shell formation rate Rsf. In order to synthesize samples with more shells, we reduce the oxygen volume in the gas, and when O_2:N_2=1:9 and 1:19, we got QS HoMSs.

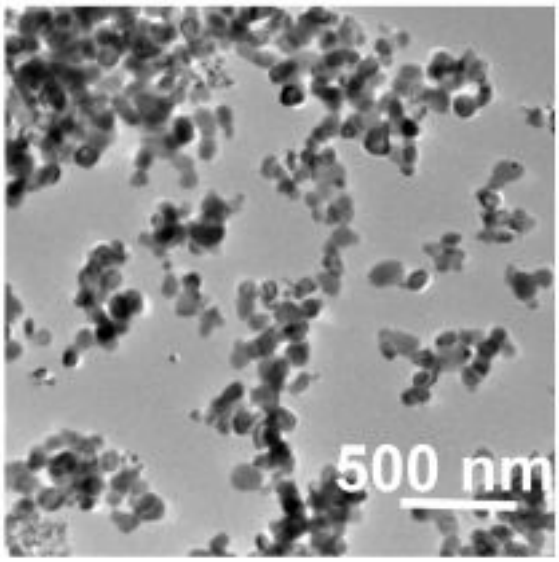

Figure S13. TEM image of QS Co_3O_4 (ZIF-67) after grinding.

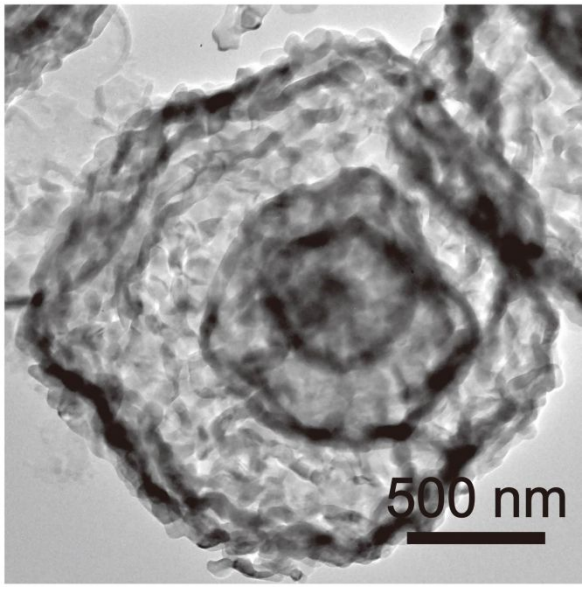

Figure S14. TEM image of QS Co_3O_4 HoMSs (CMS).

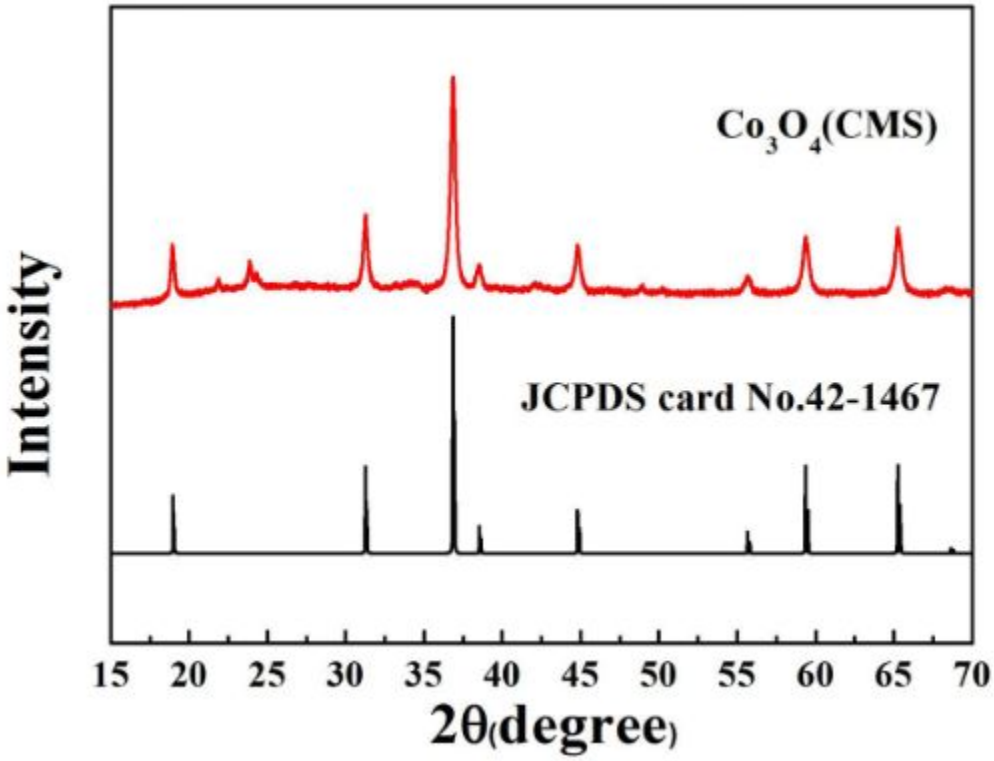

Figure S15. XRD patterns of QS Co_3O_4 HoMSs (CMS).

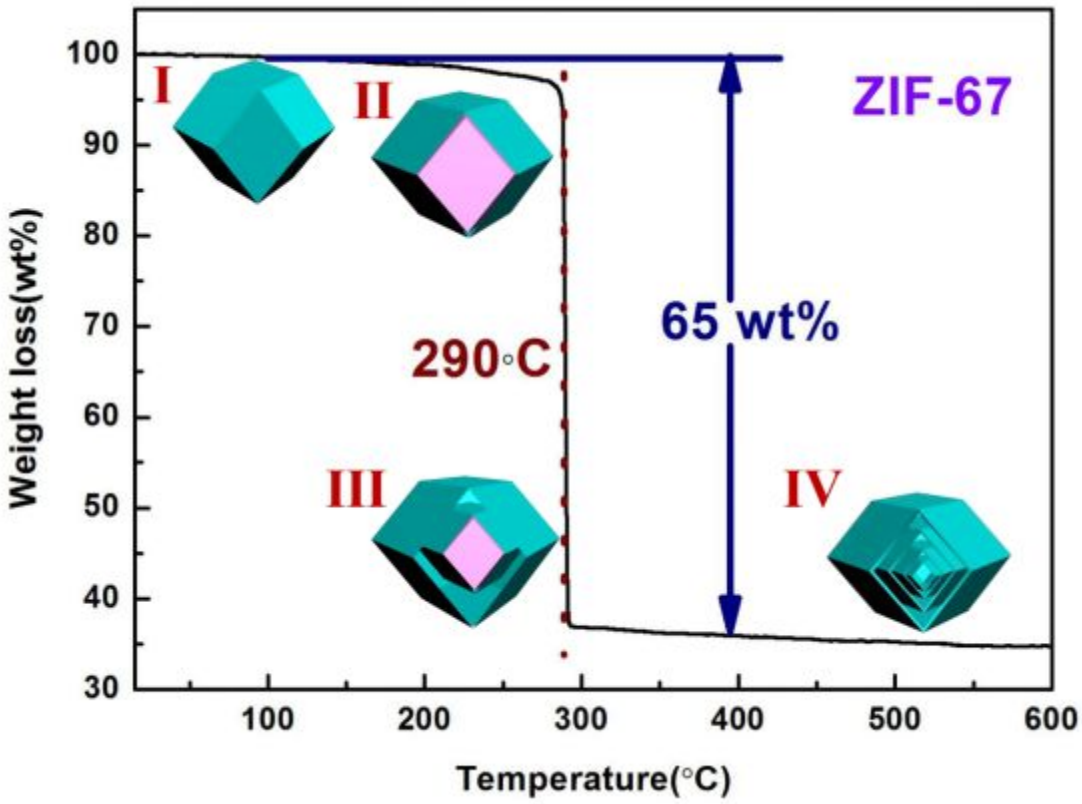

Figure S16. TGA curve of ZIF-67.

ZIF-67 had a slow weight loss between 180 and 290 °C, corresponding to the evaporation of water molecules. At 290 °C, rapid weight loss occurred, the plateau of the weight was reached after 65% weight loss, and no mass change occurred after.

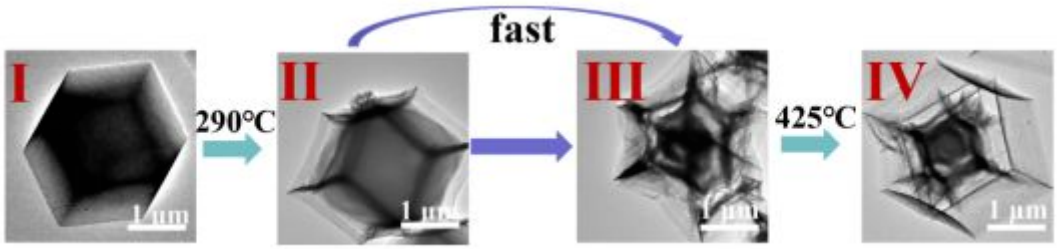

Figure S17. TEM images of samples during the reaction process, (I) ZIF-67, (II, III) 290 °C, (IV) 425 °C.

We studied the reaction process by heating 2.5 μm ZIF-67 at 0.5 °C/min to 425 °C under the gas condition of O_2:N_2=1:9, and took three temperature points, corresponding to (Ⅰ) room temperature, (Ⅱ, Ⅲ) 290 °C (Ⅳ) 425 °C, respectively. When the temperature reached 290 °C, outer layer of MOF began to decompose into Co_3O_4, and TS HoMS appear in a very short time. When the temperature rises to 425 °C, a stable QS Co_3O_4 HoMSs formed.

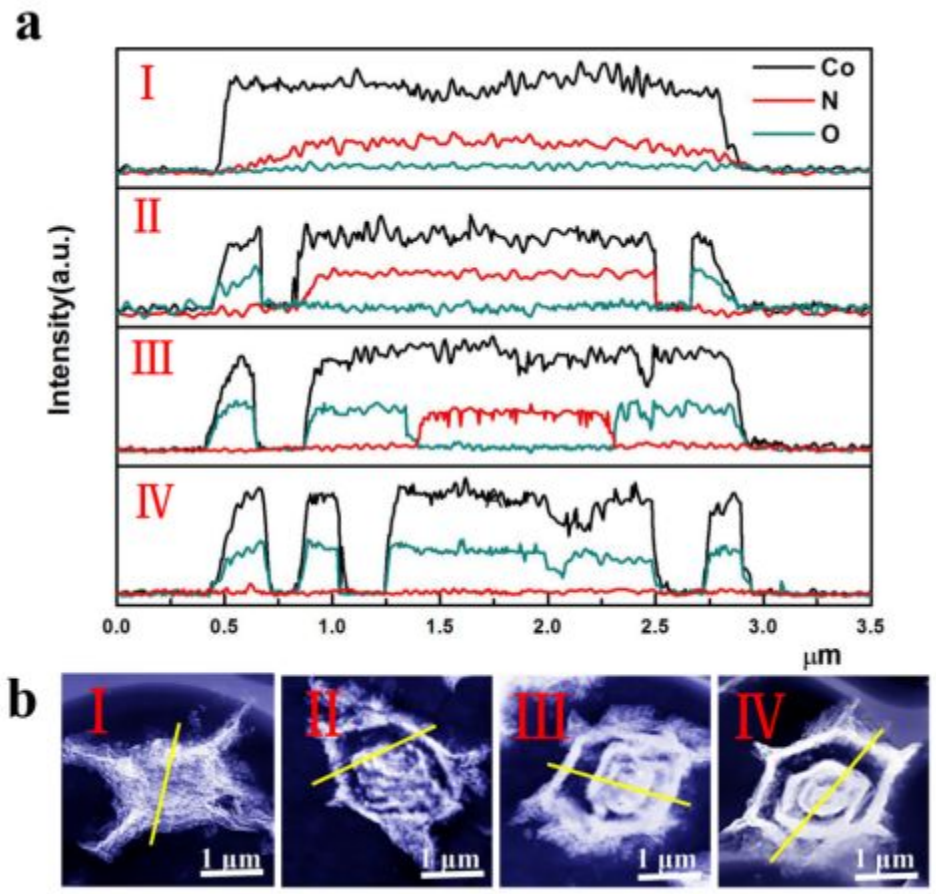

Figure S18. (a) STEM images and (b) line scanning of samples during the reaction process. ((Ⅰ) ZIF-67, (Ⅱ, Ⅲ) 290 °C (Ⅳ) 425 °C).

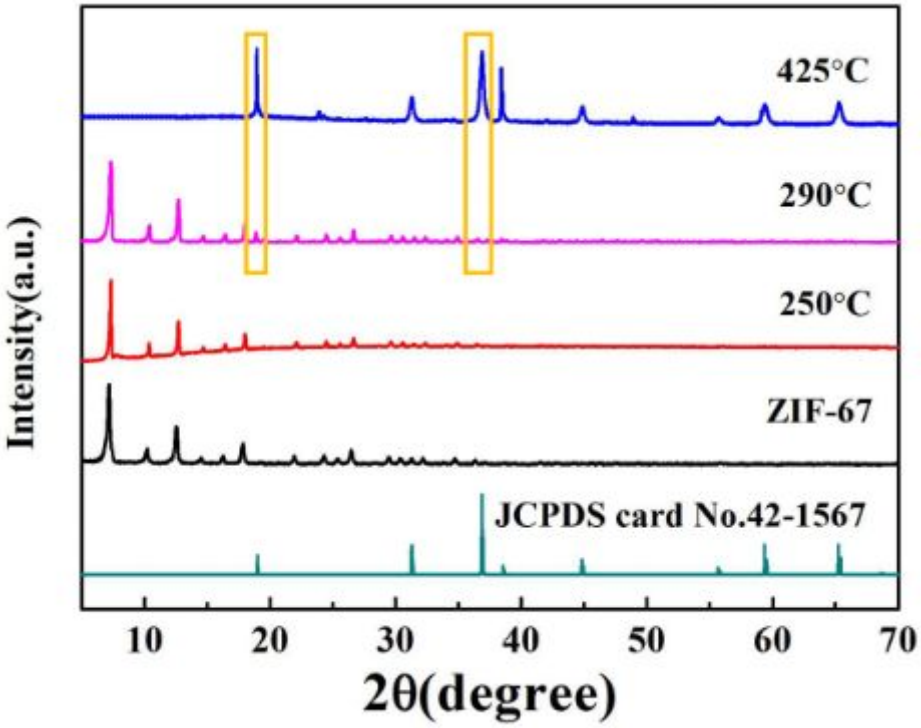

Figure S19. XRD patterns of samples during the reaction process, ZIF-67, 250 °C, 290 °C and 425 °C (for TS Co_3O_4 HoMSs).

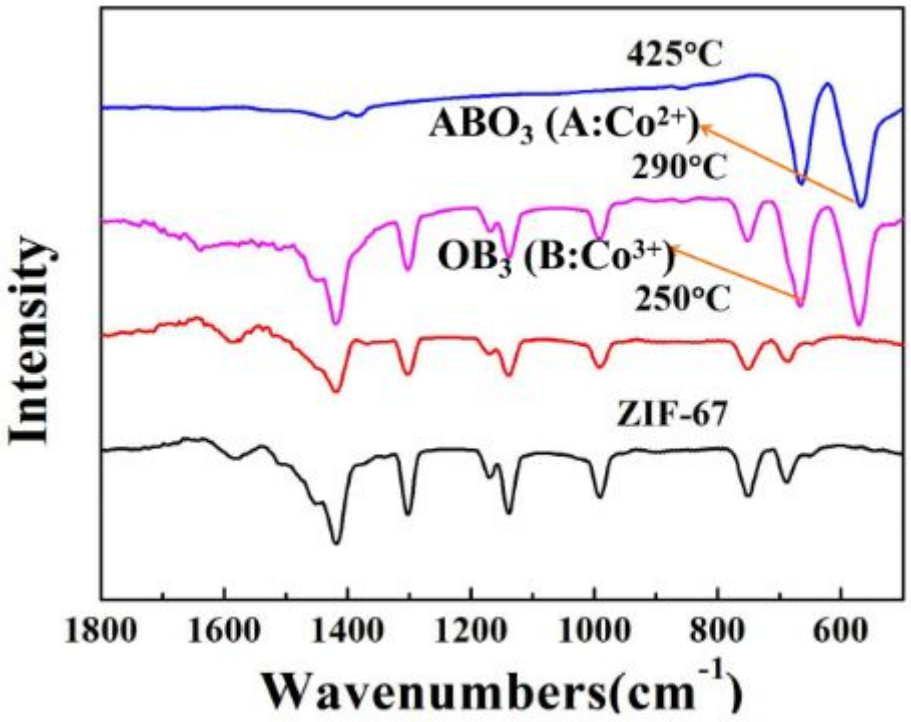

Figure S20. FT-IR spectroscopy of samples during the reaction process, ZIF-67, 250 °C, 290 °C and 425 °C.

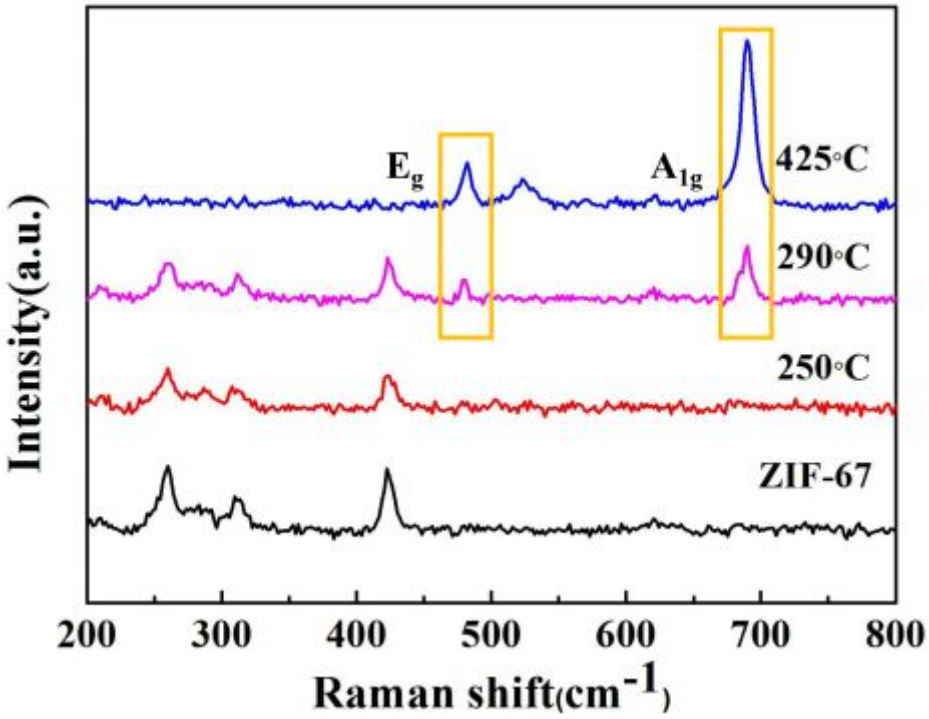

Figure S21. Raman spectroscopy of samples during the reaction process, ZIF-67, 250 °C, 290 °C and 425 °C.

Corresponding to the XRD characterization, the Raman characterization also begins to exhibit a vibrational peak of the Co-O bond at a temperature of 290 °C. The prominent Raman peaks correspond to the E_g (482 cm^{-1}) and A_{1g} (690 cm^{-1}) modes of Co_3O_4 crystalline phase.[2]

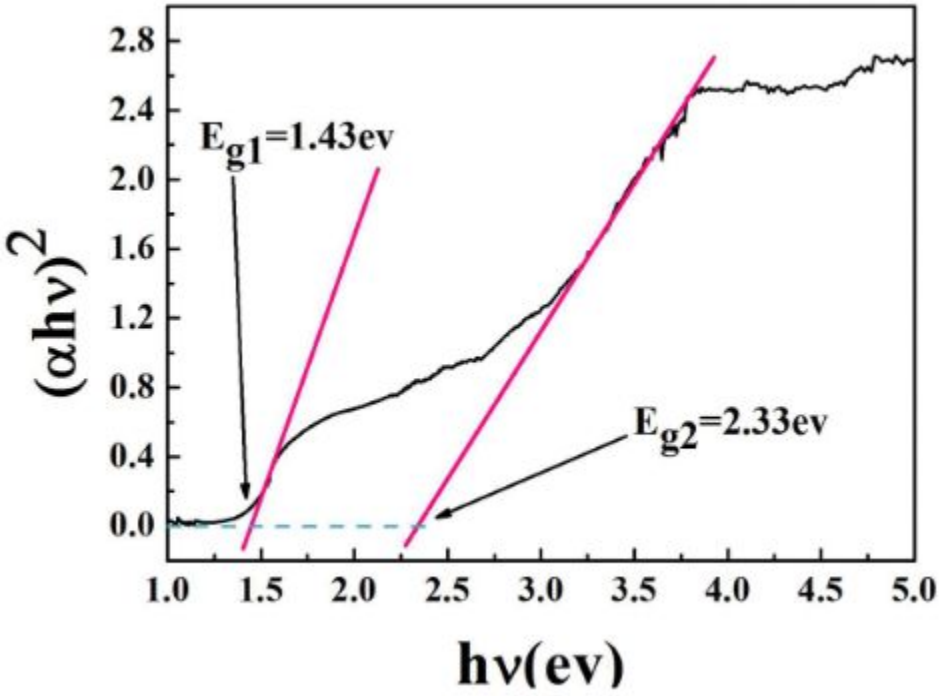

Figure S22. Tauc plot of QS Co_3O_4 (ZIF-67).

The optical band gap of QS Co_3O_4 (ZIF-67) can be estimated following $(\alpha h\nu)^{1/n}=A(h\nu-Eg)$. α represents the absorption coefficient, and h is Planck's constant, ν represents vibration frequency, Eg is the band gap of the sample, A is proportional constant, and n is related to the nature of the sample transition. As Co_3O_4 is the direct allowed transition sample, n=1/2 is used in the equation. By making a tangent to the Tauc curve, there are two intersections with the abscissa, and E_{g1} represents O^{2-}-Co^{3+} excitation.[2] So the band gap of the sample is 2.33 eV.

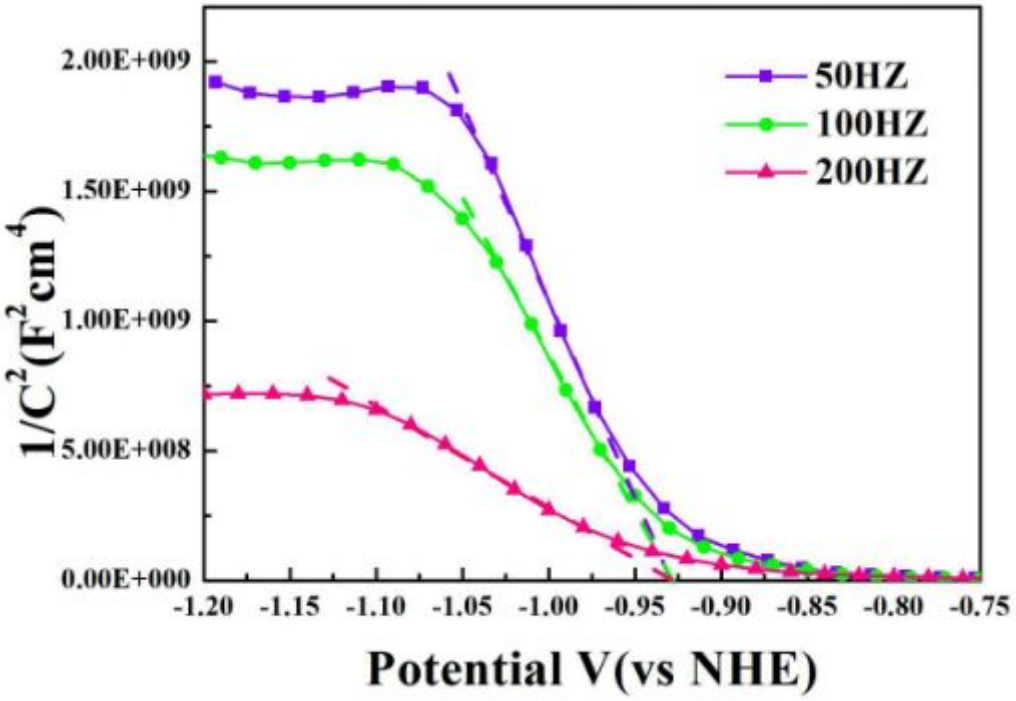

Figure S23. Mott-Schottky plot of QS Co_3O_4 (ZIF-67).

The conduction band (CB) of the material is determined by Mott-Schottky plots.

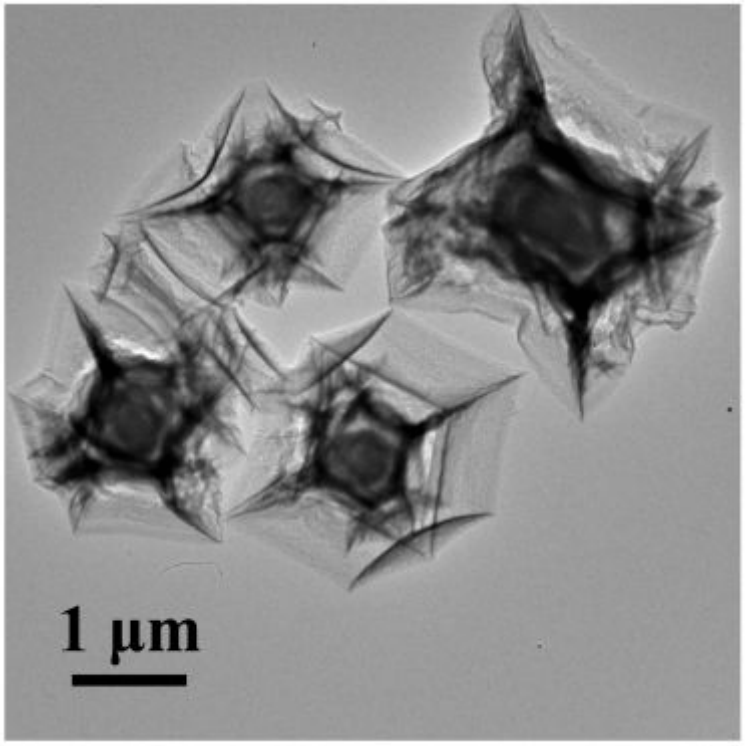

Figure S24. TEM image of QS Co_3O_4 (ZIF-67) after four circles' test.

TEM image of **Figure S24** displays the morphology of the catalysts did not change after catalytic reaction.

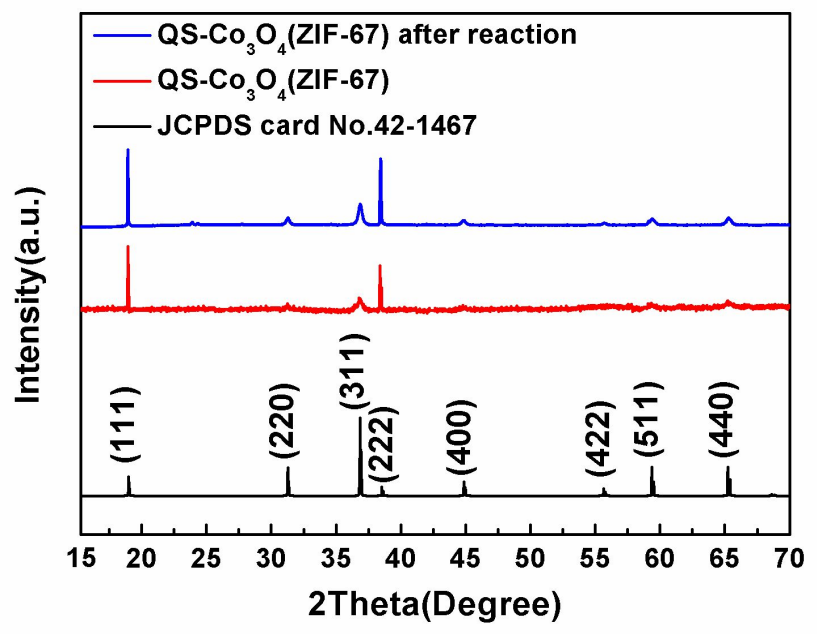

Figure S25. XRD patterns of QS Co_3O_4 (ZIF-67) before and after reaction.

XRD pattern of spent QS-Co_3O_4 HoMSs (ZIF-67) (**Figure S25**) demonstrates the same crystal structure as the original one.

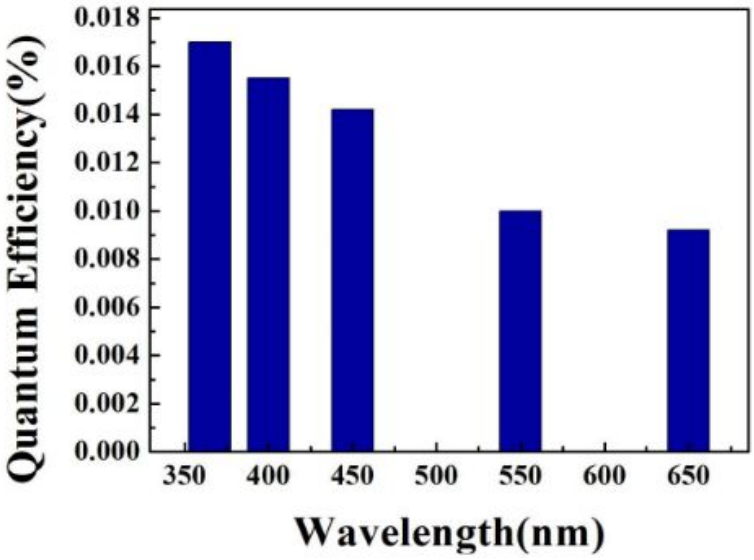

Figure S26. External quantum efficiency of QS-Co_3O_4 (ZIF-67).

Table S1. Binding energy of CS, DS, TS and QS Co_3O_4 (ZIF-67).

sample	Co^{3+} BE/ev		Co^{2+} BE/ev		Co^{2+} satellite peak BE/ev	
CS	780.63	795.75	783.1	798.3	788.4	804.5
DS	781.6	796.87	783.4	798.6	789.7	805.8
TS	783.35	798.47	785.17	800.37	791.5	807.6
QS	782.1	797.37	783.7	798.9	790.4	806.5

Table S2. The comparison of CO_2 reduction performance of cobalt oxide-based catalysts in other works.

Catalyst	Light Source	Photosensitizer	Reaction medium	Maximum production rate	Ref.
Cu/Co_3O_4	UV-Vis (Xe) (10 mW cm^{-2})	-	0.1M Na_2SO_4	6.75 $mmol \cdot L^{-1} \cdot cm^{-2}$ ($HCOO^-$)	3
Co_3O_4	λ>420 nm (Xe) (293.61 mW cm^{-2})	$[Ru(bpy)_3]Cl_2 \cdot 6H_2O$	MeCN/ TEOA/ H_2O	CO (3523 $\mu mol \cdot g^{-1} \cdot h^{-1}$)	4
$ZnO@Co_3O_4$	UV-Vis (Xe)		H_2O	CH_4 (0.99 $\mu mol \cdot g^{-1} \cdot h^{-1}$)	5
$InNbO_4/Co_3O_4$	UV-Vis (Xe) (143.61 mW cm^{-2})		$KHCO_3$	CH_3OH (1.503 $\mu mol \cdot g^{-1} \cdot h^{-1}$)	6
Co_3O_4/CeO_2	λ>400 nm (Xe)		Na_2CO_3, Na_2SO_3	CH_3OH (1.52 $\mu mol \cdot g^{-1} \cdot h^{-1}$), C_2H_5OH (4.75 $\mu mol \cdot g^{-1} \cdot h^{-1}$)	7
Co_3O_4	510nm<λ <620nm, LED (21W)		H_2O	HCOOH (4.53 $\mu mol \cdot g^{-1} \cdot h^{-1}$), HCOH (0.62 $\mu mol \cdot g^{-1} \cdot h^{-1}$), CH_3OH, CO	8
Co_3O_4	400nm<λ <1000nm, LED (5W)	$[Ru(bpy)_3]Cl_2 \cdot 6H_2O$	MeCN/ TEOA/ H_2O	CO (4.52 $\mu mol \cdot g^{-1} \cdot h^{-1}$)	9
Co_3O_4	UV-Vis (Xe) (100.61 mW cm^{-2})		H2O	MeOH	10
QS-Co_3O_4 HoMSs (ZIF-67)	AM 1.5G	-	H_2O	CO (46.3 $\mu mol \cdot g^{-1} \cdot h^{-1}$)	This work

Table S3. Analog resistance of samples corresponding to the EIS Nyquist plots.

	NPs	CS (ZIF-67)	DS (ZIF-67)	TS (ZIF-67)	QS (ZIF-67)	QS (CMS)	QS (ZIF-67) after grinding
R2 (Ω)	26.72	20.84	16.01	13.97	11.63	24.28	24.86

References:

(1) Wang, J.; Yang, N.; Tang, H.; Dong, Z.; Jin, Q.; Yang, M.; Kisailus, D.; Zhao, H.; Tang, Z.; Wang, D. Accurate Control of Multishelled Co_3O_4 Hollow Microspheres as High-Performance Anode Materials in Lithium-Ion Batteries. *Angew. Chem. Int. Ed.* **2013**, 125, 6545-6548.

(2) Chih, W. T.; Chen, B. W.; Shu, H. C. Characterization of Cobalt Oxides Studied by FT-IR, Raman, TPR and TG-MS. *Thermochim. Acta* **2008**, 473, 68-73.

(3) Shen, Q.; Chen, Z.; Huang, X.; Liu, M.; Zhao, G.; High-Yield and Selective Photoelectrocatalytic Reduction of CO_2 to Formate by Metallic Copper Decorated Co_3O_4 Nanotube Arrays. *Environ. Sci. Technol.* **2015**, 49, 5828-5835.

(4) Gao, C.; Meng, Q.; Zhao, K.; Yin, H.; Wang, D.; Guo, J.; Zhao, S.; Chang, L; He, Meng.; Li, Q.; Zhao, H.; Huang, X.; Gao, Y.; Tang, Z. Co_3O_4 Hexagonal Platelets with Controllable Facets Enabling Highly Efficient Visible-Light Photocatalytic Reduction of CO_2. *Adv. Mater.* **2016**, 28, 6485-6490.

(5) Wang, T.; Shi, L.; Tang, J.; Malgras, V.; Asahina, S.; Liu, G.; Zhang, H.; Meng, X.; Chang, K.; He, J.; Terasaki, O.; Yamauchi, Y.; Ye, J. A Co_3O_4-Embedded Porous ZnO Rhombic Dodecahedron Prepared Using Zeolitic Imidazolate Frameworks as Precursors for CO_2 Photoreduction. *Nanoscale* **2016**, 8, 6712-6720.

(6) Lee, D.; Chen, H.; Chen, Y. Photocatalytic Reduction of Carbon Dioxide with Water Using $InNbO_4$ Catalyst with NiO and Co_3O_4 Cocatalysts. *J. Phys. Chem. Solids* **2012**, 73, 661-669.

(7) Huang, Y.; Yan, C.; Guo, C.; Huang, S. Enhanced Photoreduction Activity of Carbon Dioxide over Co_3O_4/CeO_2 Catalysts under Visible Light Irradiation. *Int. J. Photoenergy* **2015**, 230808.

(8) Mendoza, J.; Kim, H.; Park, H.; Park, K. Photocatalytic Reduction of Carbon Dioxide Using Co_3O_4 Nanoparticles under Visible Light Irradiation. *Korean J. Chem. Eng.* **2012**, 29, 1483-1486.

(9) Chen, W.; Han, B.; Tian, C.; Liu, X.; Liang, S.; Deng, H.; Lin, Z. MOFs-Derived Ultrathin Holey Co_3O_4 Nanosheets for Enhanced Visible Light CO_2 Reduction. *Appl. Catal. B Environ.* **2019**, 244, 996-1003.

(10) Pocoví-Martínez, S.; Zumeta-Dube, I.; Diaz, D. Production of Methanol from Aqueous CO_2 by Using Co_3O_4 Nanostructures as Photocatalysts. *J. Nanomater.* **2019**, 6461493.